ELECTRONIC STATES OF QUANTUM DOTS

MARTA BETCKE * AND HEINRICH VOSS †

Abstract. The self-assembled quantum dots are grown on wetting layers and frequently in an array-like-assembly of many similar but not exactly equal dots. Nevertheless, most simulations disregard these structural conditions and restrict themself to simulating of a pure single quantum dot. Moreover, many simulations settle for the linear model with constant instead of the rational effective mass. In this work we argue that the nonlinear model is necessary to correctly capture the interesting part of the spectrum. We advocate the effective one electronic band Hamiltonian with the energy and position dependent effective mass approximation and a finite height hard-wall 3D confinement potential for computation of the energy levels of the electrons in the conduction band. Within this model we investigate the geometrical effects mentioned above on the electronic structure of a pyramidal InAs quantum dot embedded in a GaAs matrix. We find that the presence of a wetting layer may affect the electronic structure essentially. Furthermore, we establish that in spite of the large band gap of the InAs/GaAs heterostructure if the dots in a vertically aligned array are sufficiently close stacked there is a considerable interaction between their eigenfunctions. Moreover, the eigenfunctions of such an array are quite sensitive to certain structural perturbations.

Key words. Quantum dot, Nonlinear eigenvalue problem, Min–Max characterization, Iterative method, Electronic state

AMS subject classifications. 65F15, 65F50

1. Introduction.

Semiconductor nanostructures have attracted tremendous attention in the past few years because of their unique physical properties and their potential for applications in micro– and optoelectronic devices. Furthermore, the one electron quantum dot remains a strong candidate for implemention of a quantum computer. In semiconductor nanostructures, the free carriers are confined to a small region of space by potential barriers, and if the size of this region is less than the electron wavelength, the electronic states become quantized at discrete energy levels. The ultimate limit of low dimensional structures is the quantum dot, in which the free carriers are confined in all three directions of space. Such an energy quantization is an intrinsic property of an atom, which makes the quantum dot an interesting model for investigating the properties of systems at the atomic level.

Quantum dots can be produced today by means of the Stranski–Krastanov process which uses the relief of the elastic energy when two materials with a large lattice mismatch form an epitaxial structure. The deposited layer initially grows as a thin two dimensional (2D) wetting layer. As the deposited layer exceeds a critical thickness, the growth mode switches from 2D to 3D leading to the formation of a self-assembled quantum dot on the top of the wetting layer. If the just accrued island is subsequently completely covered with a sufficiently thick layer of the bulk matrial, the islands formed during the next deposition cycle tend to vertically correlate with the already formed layer. This leads to formation of vertically aligned arrays of quantum dots. Such a formation may be thought of as an artificial molecule and is therefore theoretically interesting for investigation of quantum mechanical coupling and transport phenomena. But vertically aligned arrays have also been used to enhance the performance of devices like quantum dot– light emmiting diodes, lasers or spectrometers, which suffer from the low gain or responsibility in presence of only one

*former Markiewicz, Institute of Numerical Simulation, Hamburg University of Technology, D-21071 Hamburg, Germany. {m.betcke}@tu-harburg.de

†Institute of Numerical Simulation, Hamburg University of Technology, D-21071 Hamburg, Germany. {voss}@tu-harburg.de

dot layer. As a product of a physical process the dots in an array can slightly differ in shape or size, hence it is an appealing problem if this may affect their electronic properties. Eventually, a new growth mode has been reported in the literature [12] involving deposition of the second layer before the dot has been completely covered by the surrounding matrial. This results in several new array forms exhibiting a strong coupling between the quantum dots.

Nevertheless, most simulations neglect the effect of the wetting layer (cf. [5, 6, 9, 10, 13, 14, 24, 25] and the literature given therein) and the coupling resulting from the vertical alignment or the alternation of size and shape of the compounds on the electronic structure of a self-assembled quantum dot. This work aims to fill this gap reporting on numerical simulations investigating how the mentioned factors influence the electronic structure of a pyramidal InAs quantum dot embedded in a GaAs matrix. We consider the one-band envelope-function formalism for electrons and holes assuming non-parabolicity for the electron's dispersion relation and an electron effective mass depending on the position and the energy level. Then the discretization of the Schrödinger equation results in a sparse eigenvalue problem depending nonlinearly on the eigenparameter. Similar experiments exploring the influence of the wetting layer are contained in [17, 18, 19, 20] where the authors assumed an axially symmetric quantum dot and an electron effective mass which does not depend on the energy level. These assumptions lead to linear eigenvalue problems of much smaller dimension. Few authors considered the vertically aligned arrays of cylindrical coaxial quantum dots [11, 15] and [7] a vertically aligned array of pyramidal quantum dots on wetting layer using the anisotropic nonparabolic effective mass approximation. The latter work investigates in the framework of a more involved model the influence of strain, piezoelectricity and indium diffusion resulting in shape and size variation of the compound dots. In contrast, our main focus is the geometrical aspect of electronic coupling. Thus we abstract from the detailed crystal properties and using a simpler but adequate model we examine more different shape abberations corresponding to the physical phenomena mentioned in the last paragraph. Moreover, the authors of [7] report that the convergence of the numerical schema IEOM scales with the inverse of the separation of the eigenvalues, which can be very close in weakly coupled systems and actually due to the symmetry there are even multiple eigenvalues. In order to obtain a satisfactory approximation to the eigenfunction they had to amend their scheme by an additional inverse iteration scheme involving a linear system solve by the biconjugate gradient method. The bad separation of the spectrum does not affect our method which efficiently computes eigenvalues and the corresponding eigenvectors to the desired accuracy using a preconditioner only as good (expensive) as the size of the problem allows for.

Our paper is organized as follows. In Section 2 we introduce the one band effective Hamiltonian which models the electronic behavior of the structures we consider i.e. a quantum dot possibly including a wetting layer, being a part of a vertically aligned structure and possibly perturbed in one of the ways described above. The corresponding rational eigenvalue problem and its basic properties are derived in Section 3. Discretization by a Galerkin method yields in all cases a sparse rational matrix eigenvalue problem which also allows a minmax characterization of its eigenvalues. Section 4 describes the iterative projection method introduced already in [25] and asserts its scope of application. Further, the solution of the projected rational eigenproblems by safeguarded iteration is expounded in detail. In Section 5 we present some numerical results demonstrating the necessity of involving the nonlinear models

as well as the effect of the wetting layer, vertical alignment and diverse shape and size perturbations on the electronic structure of a quantum dot. The conclusions and some ideas for future research are summarized in the last section.

2. Position dependent effective mass model. We consider the problem to compute relevant energy states and corresponding wave functions of three dimensional semiconductor nanostructures of the following shapes: quantum dot with and without wetting layer, quantum well, an array of vertically aligned quantum dots where as the case may arise one of the dots has been perturbed in shape or size and four stages of formation of vertically coupled quantum dots introduced in [12] cf. Figure 2.1 (e)-(h). Each of the structures is embedded in a matrix of different material. For the purpose of modeling, a bounded cuboid matrix is used. We denote by $\Omega_q, \Omega_m \subset \mathbb{R}^3$ the domain occupied by the structure and the matrix, respectively. A typical example of such a nonostructure is an InAs pyramidal quantum dot grown on a wetting layer, which is embedded in a cuboid GaAs matrix, which we will use in this paper as a basis for all the structures listed above.

We consider the one-band envelope-function formalism for electrons and holes in which the effective Hamiltonian is given by

$$\hat{H} = -\frac{\hbar^2}{2}\nabla \cdot \left(\frac{1}{m(\lambda, x)}\nabla\right) + V(x) \tag{2.1}$$

where $\hbar$ is the reduced Planck constant, and ∇ denotes the spatial gradient.

Assuming non-parabolicity for the electron's dispersion relation, the electron effective mass $m(\lambda, x)$ is constant on Ω_q and on the matrix Ω_m for every fixed energy level λ, and is taken as [1, 3]

$$\frac{1}{m_j(\lambda)} := \frac{1}{m(\lambda, x)}\bigg|_{x\in\Omega_j} = \frac{P_j^2}{\hbar^2}\left(\frac{2}{\lambda + E_{g,j} - V_j} + \frac{1}{\lambda + E_{g,j} - V_j + \Delta_j}\right), \tag{2.2}$$

for $j \in \{m, q\}$, where the confinement potential $V_j := V|_{\Omega_j}$ is piecewise constant, and P_j, $E_{g,j}$ and Δ_j are the momentum matrix element, the band gap, and the spin-orbit splitting in the valence band for the quantum dot material ($j = q$) and the matrix ($j = m$), respectively.

To determine the relevant energy states and corresponding wave functions ϕ we have to solve the governing stationary Schrödinger equation

$$-\nabla \cdot \left(\frac{\hbar^2}{2m_j(\lambda)}\nabla\phi\right) + V(x)\phi = \lambda\phi, \quad x \in \Omega_q \cup \Omega_m. \tag{2.3}$$

The relevant energy levels are the eigenvalues smaller than the confinement potential. These are also called confined states since the corresponding wave functions mainly live on the quantum dot(s) and eventually wetting layer(s) and rapidly decay outside of the structure. Thus it is reasonable to assume homogeneous Dirichlet conditions $\phi = 0$ on the outer boundary of the matrix as long as the wetting layer is not present. In the latter case the homogeneous Dirichlet boundary conditions are still applicable on the top and the bottom of the matrix ($\partial\Omega_h$) but not any more on the side walls ($\partial\Omega_v$), which cut through the wetting layer. In [17] the authors suggest to use the homogeneous Neumann boundary conditions $\frac{\partial\phi}{\partial n} = 0$ on the side walls of the matrix. We follow this idea as it can be neatly motivated by considering the quantum dot on the wetting layer as a small perturbation of the latter one. Therefore the functions

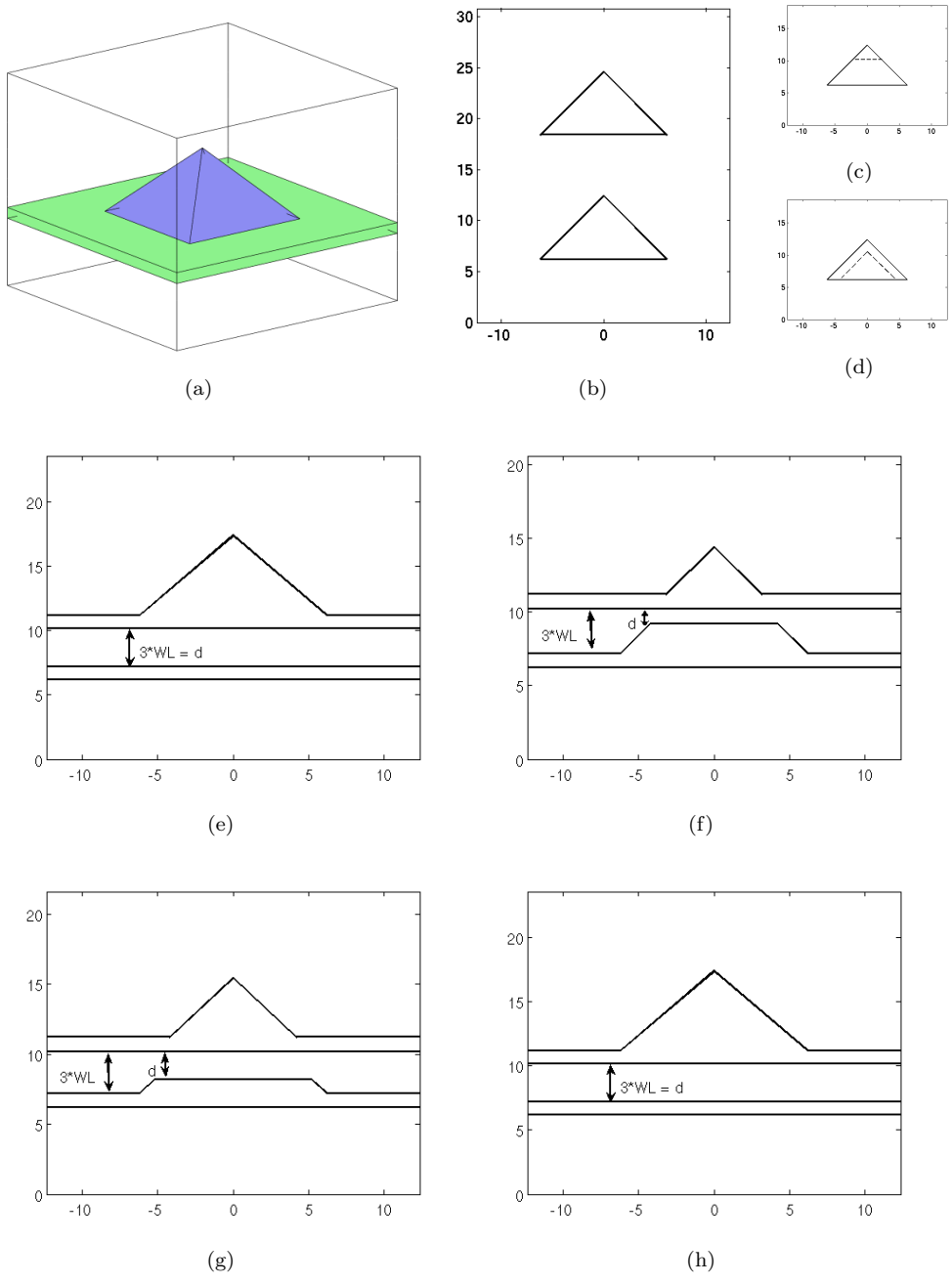

FIG. 2.1. *(a) Quantum dot (blue) with wetting layer (green), (b) an array of vertically aligned quantum dots (c) truncated dot (d) scaled dot (e)-(h) four vertically coupled quantum dots on wetting layer of thickness 1 nm , d = 0, . . . , 3 nm*

far away from the dot should approach those from the pure wetting layer. Moreover, if we assume the wetting layer to be infinite in both the x and y direction, it becomes a quantum well, a one dimensional structure along the z axis. Therefore the eigenfunctions of such a quantum well do not depend on x and y, $\phi(x,y,z) = \phi(z)$ and so do not their derivatives. Since, it holds in every point of space

$$\frac{\partial \phi(x,y,z)}{\partial x} = \frac{\partial \phi(x,y,z)}{\partial y} = 0,$$

so especially on the boundary $\partial\Omega_v$. As we have seen the Neumann boundary conditions on the sidewalls of the matrix simulate the physically generic case of an infinite wetting layer, hence they are a consistent and reasonable constraints to pose on the solution.

On the interface between the quantum structure material and the matrix the Ben Daniel–Duke condition [8] holds

$$\frac{1}{m_q}\,\frac{\partial \psi}{\partial n_q}\bigg|_{\partial\Omega_q} = \frac{1}{m_m}\,\frac{\partial \psi}{\partial n_m}\bigg|_{\partial\Omega_m}, \quad x \in \partial\Omega_q \cap \partial\Omega_m. \tag{2.4}$$

Here n_q and n_m denote the outward unit normal on the boundary of Ω_q and Ω_m, respectively.

3. Nonlinear eigenvalue problem. In this section we derive the nonlinear eigenvalue problem resulting from the energy dependent effective mass model described in the last section. Let $\Omega := \bar{\Omega}_q \cup \Omega_m$ and $H := \{\psi \in H^1(\Omega) : \psi = 0 \text{ on } \partial\Omega_h\}$, where $H^1(\Omega)$ denotes the usual Sobolev space. Multiplying equation (2.3) by $\phi \in H$ and integrating by parts, one gets the variational form of the Schrödinger equation

$$\begin{aligned} a(\psi,\phi;\lambda) := {} & \frac{\hbar^2}{2m_q(\lambda)} \int\limits_{\Omega_q} \nabla\psi \cdot \nabla\phi \, dx + \frac{\hbar^2}{2m_m(\lambda)} \int\limits_{\Omega_m} \nabla\psi \cdot \nabla\phi \, dx + V_q \int\limits_{\Omega_q} \psi\phi \, dx \\ & + V_m \int\limits_{\Omega_m} \psi\phi \, dx = \lambda \int\limits_{\Omega} \psi\phi \, dx =: \lambda b(\psi,\phi) \quad \text{for every } \phi \in H. \end{aligned} \tag{3.1}$$

In a similar way as in [25] it can be shown, that problem (3.1) has a countable set of positive eigenvalues $0 < \lambda_1 \le \lambda_2 \le \cdots \to \infty$ of finite multiplicity which satisfy a minmax characterization. Namely, for fixed $\psi \neq 0$ the real equation

$$f(\lambda;\psi) := \lambda b(\psi,\psi) - a(\psi,\psi;\lambda) = 0 \tag{3.2}$$

has a unique positive solution $p(\psi)$. Hence, equation (3.2) defines a functional $p : H \setminus \{0\} \to \mathbb{R}$ called Rayleigh functional (which generalizes the Rayleigh quotient for linear eigenproblems), and the kth smallest eigenvalue of (3.1) satisfies

$$\lambda_k = \min_{\dim V = k} \max_{u \in V, u \neq 0} p(u). \tag{3.3}$$

Moreover, an eigenvalue $\tilde{\lambda}$ of (3.1) is the kth smallest eigenvalue if and only if $\mu = 0$ is the kth largest eigenvalue of the linear eigenvalue problem

$$\tilde{\lambda} b(\psi,\phi) - a(\psi,\phi;\tilde{\lambda}) = \mu b(\psi,\phi) \quad \text{for every } \phi \in H. \tag{3.4}$$

Discretizing the Schrödinger equation (2.3) with the boundary and interface conditions specified above by a Galerkin method (finite elements, e.g.) one gets a rational matrix eigenvalue problem

$$S(\lambda)x := \lambda Mx - \frac{1}{m_q(\lambda)}A_q x - \frac{1}{m_m(\lambda)}A_m x - Bx = 0 \tag{3.5}$$

where

$$A_j = \Big(\int\limits_{\Omega_j} \nabla\phi_k \cdot \nabla\phi_\ell \, dx\Big)_{k,\ell},\ j \in \{q, m\}$$

$$M = \Big(\int\limits_{\Omega} \phi_k\phi_\ell \, dx\Big)_{k,\ell} \quad \text{and} \quad B = \Big(V_q \int\limits_{\Omega_q} \phi_k\phi_\ell \, dx + V_m \int\limits_{\Omega_m} \phi_k\phi_\ell \, dx\Big)_{k,\ell}$$

and ϕ_i denotes a basis of the ansatz space.

A_q, A_m and B are symmetric and positive semi–definite, and M is positive definite, and for $\lambda \geq 0$ the matrix

$$\frac{\hbar^2}{2m_q(\lambda)}A_q + \frac{\hbar^2}{2m_q(\lambda)}A_q$$

is positive definite. Hence, the eigenvalues of the discretized problem (3.5) satisfy a minmax principle as well, and it follows from the minmax characterization (3.3) of the nonlinear Schrödinger equation that the kth smallest eigenvalue of the discretized problem (3.5) is an upper bound of the corresponding eigenvalue of problem (2.3).

4. Solving the discretized problem. In this section we consider the problem to compute a few eigenvalues and corresponding eigenvectors at the lower end of the spectrum of the discretization (3.5) of the Schrödinger equation (2.3).

For linear sparse eigenproblems $S(\lambda) = \lambda B - A$ very efficient methods are iterative projection methods like the Lanczos, the Arnoldi, and the Jacobi–Davidson method, e.g., where approximations to the wanted eigenvalues and eigenvectors are obtained from projections of the eigenproblem to subspaces of small dimension which are expanded in the course of the algorithm.

Let $V \in \mathbb{R}^{n\times k}$ be an (orthonormal) basis of the current search space $\mathcal{V} \subset \mathbb{R}^n$, and assume that $(\theta, y), y \in \mathbb{R}^k$ is an eigenpair of the projected eigenvalue problem

$$V^T S(\lambda) V y = 0, \tag{4.1}$$

and denote by $x := Vy$ the corresponding Ritz vector. To obtain an improved approximation it is reasonable to expand $\mathcal{V}$ by a direction with a high approximation potential for the eigenvector wanted next.

There are two approaches in the literature for expanding the search space, both approximating inverse iteration: a Jacobi–Davidson type method [2] and the Arnoldi method [23] based on the residual inverse iteration. Here we restrict ourselves to the latter one.

Residual inverse iteration (introduced by Neumaier [21]) suggests the expansion

$$v = S(\sigma)^{-1}S(\theta)x, \tag{4.2}$$

of the search space $\mathcal{V}$, where σ is a fixed parameter close to the wanted eigenvalues.

For a linear eigenproblem $S(\lambda) = A - \lambda B$ this is exactly the Cayley transform with pole σ and zero θ, and since $(A - \sigma B)^{-1}(A - \theta B) = I + (\sigma - \theta)(A - \sigma B)^{-1}B$ and Krylov spaces are shift-invariant the resulting projection method expanding $\mathcal{V}$ by v is nothing else but the shift-and-invert Arnoldi method.

If the linear system $S(\sigma)v = S(\theta)x$ is too expensive to solve for v we may choose as new direction $v = K^{-1}S(\theta)x$ with $K \approx S(\sigma)$, and for the linear problem we obtain an inexact Cayley transform or a preconditioned Arnoldi method. The resulting iterative projection method given in Algorithm 1 therefore is called nonlinear Arnoldi method, although no Krylov space is constructed and no Arnoldi recursion holds.

Algorithm 1 Nonlinear Arnoldi Method

start with an initial pole σ and an initial orthonormal basis V, $V^TV = I$
determine preconditioner $K \approx S(\sigma)$, σ close to the smallest eigenvalue
k=1
while $k \leq$ number of wanted eigenvalues **do**
  compute the kth smallest eigenvalue μ and corresponding normalized eigenvector y of the projected problem $V^TS(\mu)Vy = 0$
  determine Ritz vector $u = Vy$ and residual $r = S(\mu)u$
  if $\|r\| < \varepsilon$ **then**
    accept eigenvalue $\lambda_k = \mu$, and eigenvector $x_k = u$,
    choose new pole σ and update preconditioner $K \approx S(\sigma)$ if indicated
    restart if necessary
    $k = k + 1$
  end if
  solve $Kv = r$ for v
  $v = v - VV^Tv$,$\tilde{v} = v/\|v\|$, $V = [V, \tilde{v}]$
  reorthogonalize if necessary
end while

There are many details that have to be considered when implementing the nonlinear Arnoldi method concerning the choice of the initial basis, when and how to update the preconditioner, and how to restart the method. A detailed discussion is given in [23].

A crucial point in iterative projection methods for general nonlinear eigenvalue problems when approximating more than one eigenvalue is to inhibit the method from converging to the same eigenvalue repeatedly. For linear eigenvalue problems this is easy to do by using Schur forms or generalized Schur forms for the projected problem and then locking or purging certain eigenvectors. For nonlinear problems, however, such Schur forms do not exist and this presents one of the most difficult tasks in achieving good convergence.

For symmetric nonlinear eigenproblems satisfying a minmax characterization however, its eigenvalues can be computed safely one after the other. The minimum in (3.3) is attained by the invariant subspace of $S(\lambda_k)$ corresponding to the kth largest eigenvalues, and the maximum by every eigenvector corresponding to the eigenvalue 0. This suggests the safeguarded iteration for computing the kth smallest eigenvalue which is presented in Algorithm 2 for the projected eigenproblem $P(\lambda)y := V^TS(\lambda)Vy = 0$:

The safeguarded iteration has the following convergence properties [22]: It converges globally to the smallest eigenvalue λ_1. The (local) convergence to simple eigen-

Algorithm 2 Safeguarded iteration

1: Start with an approximation μ_1 to the k-th smallest eigenvalue of $P(\lambda)y = 0$
2: **for** $\ell = 1, 2, \ldots$ until convergence **do**
3: determine an eigenvector u corresponding to the kth largest eigenvalue of the matrix $P(\mu_\ell)$
4: evaluate $\mu_{\ell+1} = p(u)$, i.e. solve $u^T P(\mu_{\ell+1})u = 0$ for $\mu_{\ell+1}$
5: **end for**

values is quadratic. If $P'(\lambda)$ is positive definite, and u in Step 3 of Algorithm 2 is replaced by an eigenvector of $P(\mu_\ell)u = \mu P'(\mu_\ell)u$ corresponding to the kth largest eigenvalue, then the convergence is even cubic. Moreover, a variant exists which is globally convergent also for higher eigenvalues.

5. Numerical experiments. A basic building block in our examples is a pyramidal quantum dot of width 12.4 nm and height 6.2 nm embedded in a cuboid matrix of size 24.8 nm×24.8 nm×18.6 nm. We consider the following structures:

1. a pure quantum dot;
2. a quantum dot on wetting layer of thinkness 1nm and 2nm;
3. a quantum well of thickness 1nm;
4. a vertically aligned array of two quantum dots;
5. an array from 4. but, where the tip of one of the dots has been truncated relatively to the dot's original height by $0.1 \ldots 0.5$;
6. as before, but with one of the dots scaled by the factor $0.9 \ldots 0.5$;
7. four different stages of the formation of vertically coupled quantum dots in Figure 2.1 (e)-(h).

All the experiments in points 4–6 we carried out also including the wetting layer. In all cases we could observe the same phenomena as without the wetting layer. But, as we will shortly see, wetting layers considerably increase the number of the confined states. Thus for the sake of clarity we decided to restrict ourself to the results obtained excluding the wetting layer since they equally well bring out the points we would like to stress.

In our examples we assume an InAs/GaAs heterojunction and for the nonparabolic effective mass approximation we used following [14] the semiconductor band structure parameters $P_q = 0.7509$, $g_q = 0.42$, $\delta_q = 0.48$, and $V_q = 0$ for InAs, and $P_m = 0.7848$, $g_m = 1.52$, $\delta_m = 0.34$, and $V_m = 0.77$ for GaAs.

Using FEMLAB [4] we discretized the Schrödinger equation by the finite element method with quadratic Lagrangian elements on a tetrahedral grid. The physically interesting energy levels are the ones which are confined to the dot. Since the envelope functions are mainly concentrated on the quantum dot (e.g. for a single pyramid it occupies only less than 3 % of Ω) and the wetting layer, and since they decay very rapidly outside the quantum dot/wetting layer structure, we chose a non-uniform grid, which is the finest on the dot-matrix interface, fine on the dot and wetting layer and quite coarse on the matrix.

To motivate the incorporation of the nonlinearity into the governing Schödinger equation we compute the energy states of a pure quantum dot for the constant effective masses and compare them with the energy levels obtained from the nonlinear Schrödinger equation. To avoid the nonlinear dependence on the energy level most simulations replace $m_j(\lambda)$ by the band edge effective mass $m_j^* = m_j(V_j)$. This translates to $m_{InAs}^* = 0.023m_0$ and $m_{GaAs}^* = 0.067m_0$, where m_0 is the free electron mass.

The energy dependence of the effective masses for InAs and GaAs is displayed in the Figure 5.1. It is apparent that the range of the attained values is too large to expect the constant effective mass to capture it correctly. In fact not even the number of confined states in both cases agrees. The linear model has only three confined states: ground state 0.3947 and the excited state 0.6451, which is an eigenvalue of multiplicity 2, while the nonlinear model has seven eigenvalues smaller than 0.77, and the ground state is by about 7% and the first excited state by 18% smaller than those of the linear approximation. The eigenvalues of the linear problem are larger than the corresponding eigenvalues of the nonlinear problem. This is not suprising, since the effective mass for the dot material has been replaced by its lower bound. And since the wave functions live mostly on the dot, this is a decisive simplification leading to an overestimation of the eigenvalues.

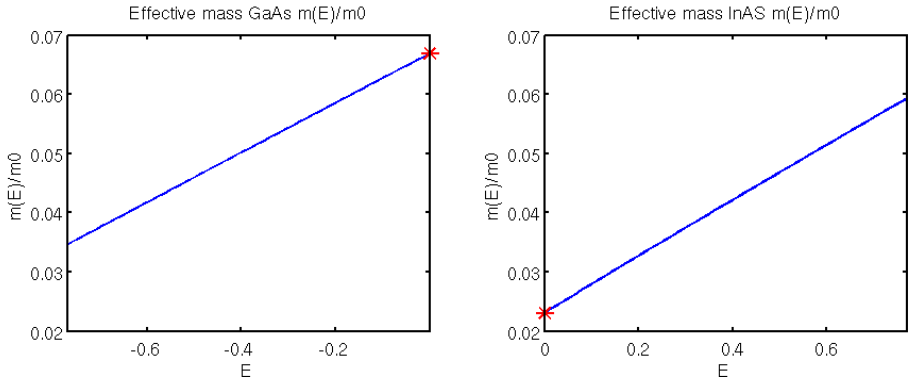

FIG. 5.1. *Effective mass*

The incipient experiment demonstrates the necessity of using a more sophisticated model than just a constant effective mass approximation. So from now on we focus on the nonlinear model introduced in Section 2. The arising rational eigenvalue problems were solved under MATLAB 7.1.0 on an Intel Pentium D processor with 4 GByte RAM and 3.2 GHz by the nonlinear Arnoldi method with incomplete LU with threshold 0.01 as a preconditioner, where the projected eigenproblems were solved by the safeguarded iteration. We started the method with a constant vector on $\overline{\Omega}_q \cup \Omega_m$ which is far away from an eigenvector, and we terminated the iteration for an eigenvalue, if the residual norm was less than 10^{-6}. Some of the analyzed structures (especially those including wetting layer), have quite a large number of confined states. In such cases, to prevent the search subspace to grow prohibitively large we restarted the algorithm, whenever the size of the search subspace excluding the already found eigenvectors exceeded 150. On restart we include 5 more vectors having a large approximating potential to the next wanted eigenvectors. Due to the symmetry of the problem there exist multiple eigenvalues (for instance the second eigenvalue for the case of dot/wl). The Arnoldi method had no problems to detect these multiple eigenvalues with the right multiplicity.

First, we consider the pure quantum dot problem which has 7 energy eigenvalues smaller than the confinement potential $V_m = 0.77$ displayed in the second column of Table 5.1. The discretized problem has 70276 degrees of freedom, and it takes 90 seconds to solve it. The envelope functions ϕ_j corresponding to these states are essentially confined to the quantum dot. The left column of Figure 5.2 shows a choice

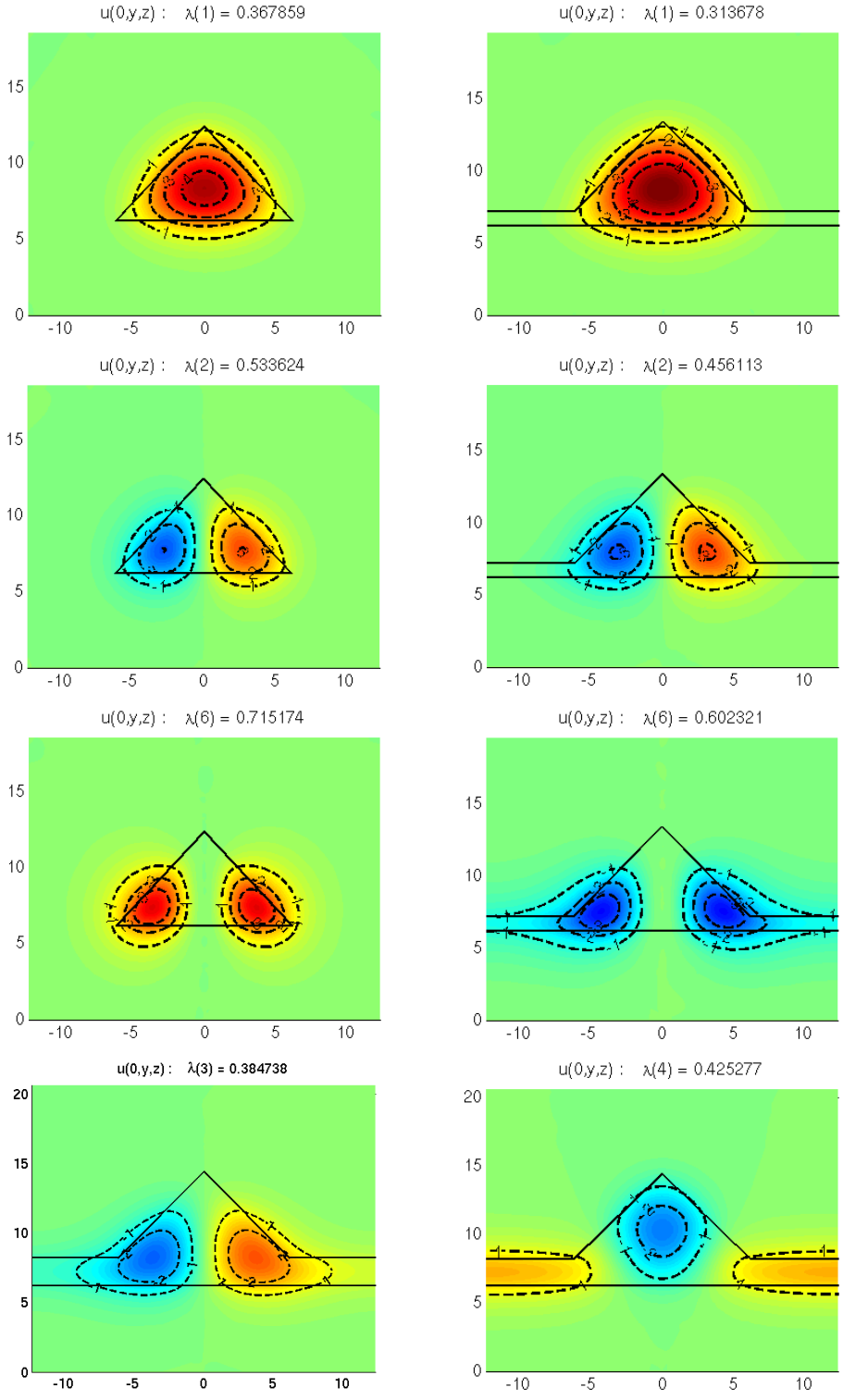

FIG. 5.2. *Envelope functions of pure quantum dot (1–3 in the left column), including 1 nm wetting layer (1–3 in the right column) and including 2nm wetting layer (last row)*

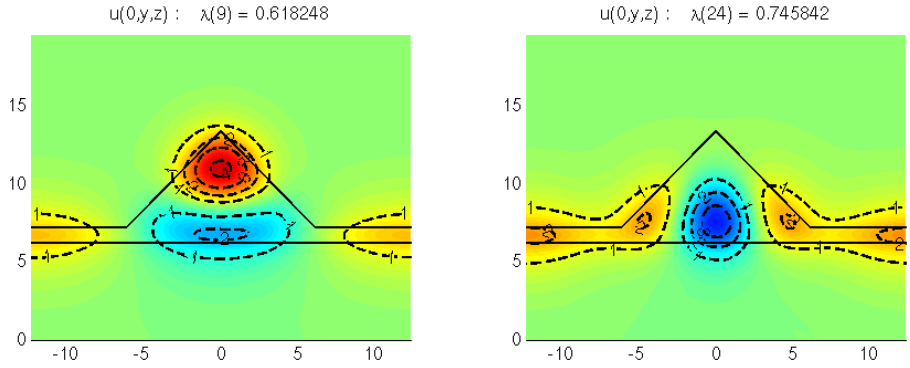

FIG. 5.3. *Envelope functions of 9th and 24th state of quantum dot on wetting layer of thickness 1 nm as a function of their distance*

of cuts $\{\phi_j(0,y,z) : (0,y,z) \in \overline{\Omega}\}$ through envelope functions ϕ_j for $j = 1, 2, 6$. ϕ_3 is obtained from ϕ_2 rotating it by 90 degrees around the z-axis.

TABLE 5.1
Electronic eigenstates

	pure QD	QD/WL 2 nm	QD/WL 1nm	pure WL 1 nm
dimension	70276	64077	65181	9758
CPU [s]	90.08	87.45	100.35	7.69
λ_1	0.3679	0.2695	0.3137	0.6050
$\lambda_{2/3}$	0.5336	0.3847	0.4561	0.6149
λ_4	0.6462	0.4253	0.5494	0.6246
λ_5	0.6538	0.4375	0.5569	0.6437
λ_6	0.7152	0.4465	0.6023	0.6437
λ_7	0.7471	0.4465	0.6150	0.6531

Next, we emend the quantum dot by a wetting layer of thickness 1 nm and 2 nm, respectively. In this case there are 27 and 44 eigenvalues smaller than V_m, respectively, The smallest 7 eigenvalues are shown in columns 3 and 4 in Table 5.1. They are substantially smaller than the corresponding ones of the pure quantum dot. For instance, the ground state is smaller by 15% and 27% and the first excited state by 15% and 28%, respectively. For the comparison the pure wetting layer of these thicknesses has 20 and 37 confined states, respectively. The envelope functions ϕ_1, ϕ_2, ϕ_6 for the case of a wetting layer of thickness 1 nm and ϕ_2, ϕ_4 for 2nm are displayed in Figure 5.2 in the right column and in the last row, respectively. While the ground state is localized quite well to the quantum dot, this property gets lost for excited eigenstates. For the wetting layer of thickness 2 nm this is even more pronounced. Once the energy level approximately reaches the ground state of the quantum well the envelope functions begin to live on the wetting layer too. This happens for the 4th eigenstate ϕ_4 for 2nm wetting layer and for the 6th ϕ_6 for 1nm. Furthermore, most of the higher energy states are some combinations of the wetting layer states with the pure dot states (cf. Figure 5.3). The presented example demonstrates that models neglecting the influence of the wetting layer can yield incorrect electronic levels.

Now, we examine the coupling between the dots on an example of a vertically aligned array of two quantum dots without wetting layers. We consider few different distances in range 0–8 nm between the dots. For contacting dots we count 13 confined states while if the dots are 1 nm and more apart 14 confined states exist. Figure 5.4 shows the dependence of the confined energy levels on the distance between the dots. For large distances between the dots the energy levels of the array approach those of a single dot, with the difference that each level is doubled. While when the gap decreases the energy levels split in the way shown in Figure 5.4. This indicates that if dots are sufficiently close to each other the energy levels become coupled by the interaction of the wave functions (cf. ground states in Figure 5.5). In that case it is necessary to simulate a whole array instead of the single dot. As shown in Figure 5.4 the coupling may lead for instance to swapping of some higher energy levels e.g. 8th and 9th (q.v. Figure 5.5 the rightmost column). Figure 5.5 shows in the first column ϕ_1 for 1nm and 6nm gaps between the dots, respectively. Since the first eigenvalue is always simple, regardless of the size of the gap between the dots a new second energy state is introduced (cf. middle column Figure 5.5). As mentioned before, we performed the same experiments including wetting layers and observed qualitatively the same behavior.

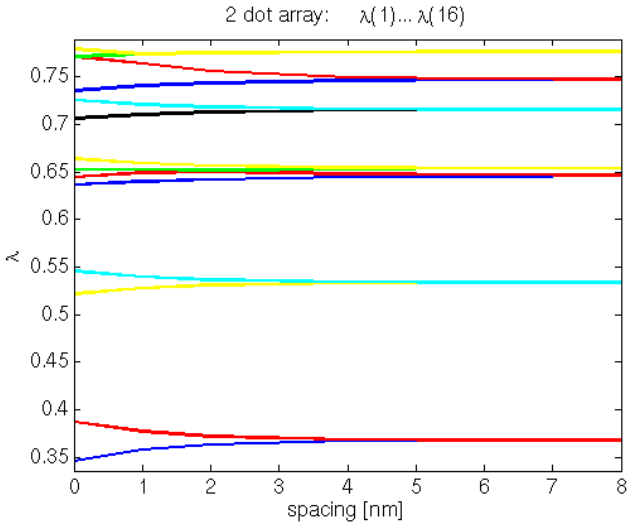

FIG. 5.4. *Energy level coupling in a vertically aligned array of two quantum dots without wetting layers*

The following examples explore the coupling of electronic states in a vertically aligned array of closely spaced dots. We consider the array from the last paragraph with 1 nm gap between the dots and we perturb one of the dots by alteration of its shape or size. First we truncate the tip of the lower pyramid. Figure 5.6 shows the dependence of the confined energy levels on the size of the truncated part of the pyramid. We can see that removing a small bit of the dot's top does not significantly change the energy levels, but the change becomes perceptible while we cut more and more off. This is not surprising since the envelope functions live mostly on the center of the pyramid and are hardly affected by removing a small bit of the tip. Though for large truncations some changes may be observed. Due to the unsymmetry of the dots, the eigenfunctions become localized (cf. Figure 5.8 1st, 2nd (partly) 7th, 10th

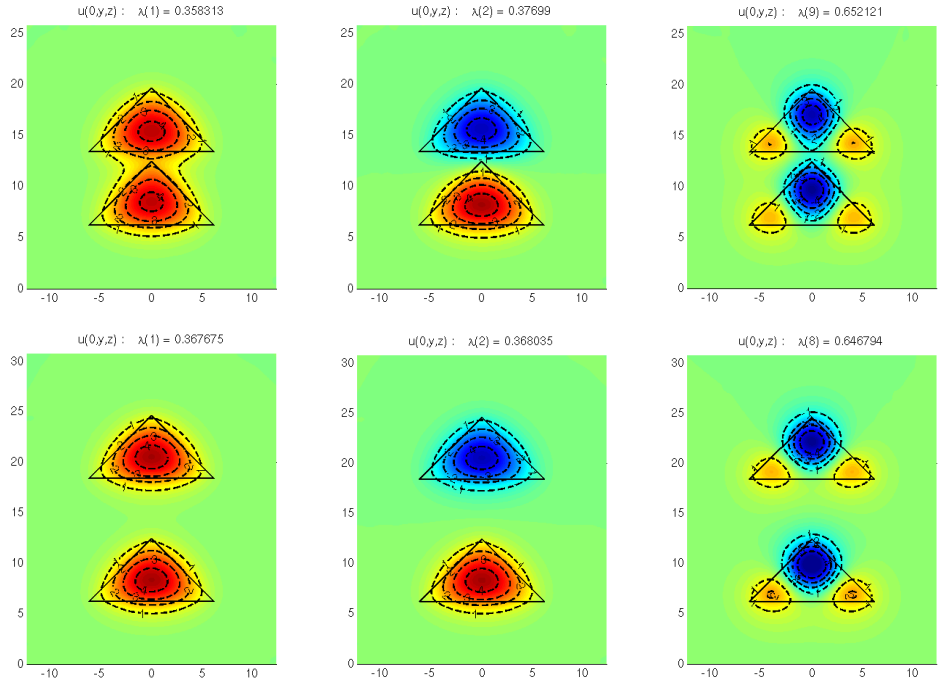

FIG. 5.5. *Envelope functions of a vertically aligned array of two dots at the distance 1 nm (first row) and 6nm (second row)*

(almost)) and approach those of a single dot. This alters the energy levels and may even lead to their interchange (e.g. 9th and 10th in Figure 5.6). The low symmetry of the pyramid justifies the question what happens when we perturb the upper dot in an array. Done so, we find that the energy levels remain almost unchanged while the eigenfunctions behave almost symmetrically. Only for large truncation a very small difference can be observed for the first and second energy level. Actually, this become first noticeable while examining the corresponding envelope functions, which exhibit slightly different coupling due to the different geometry (see 1st and 2nd state in Figure 5.8).

Now, we perturb the lower dot by scaling. In this case we observe much stronger dependence on the scaling parameter than it was for the truncation. Figure 5.7 shows that already a small change in size causes a large change of the energy levels. As for the truncation before we repeat the same experiment but now we scale the upper dot. Though, as before, most of the energy levels remain the same, slight differences in the envelope functions are perceptable already for minor scaling by 0.9 (cf. 2nd eigenstates in the leftmost column in Figure 5.9). Those become more obvious for major scaling by 0.6 (4th eigenstates in the middle column in the same figure). In both cases already exiguous variation of size entails a localization of the eigenfunctions. For scaling by 0.9 there are 12 confined states, 2 less than in the case of the original array. While the sizes of both compound dots do not differ much, the eigenfunctions localize alternatingly to one of the dots (e.g. 4th and 6th eigenstate in the rightmost column in Figure 5.9). With rising size discrepancy, the number of confined states decreases e.g. for 0.6 value of the scaling parameter there are only 8 confined states, which is

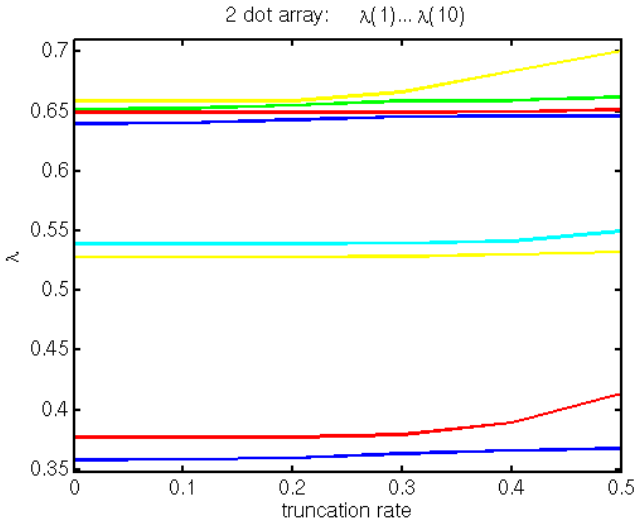

FIG. 5.6. *The energy levels of a vertically aligned array of two quantum dots at 1 nm distance, the lower one with truncated tip, in dependence of the rate of truncation*

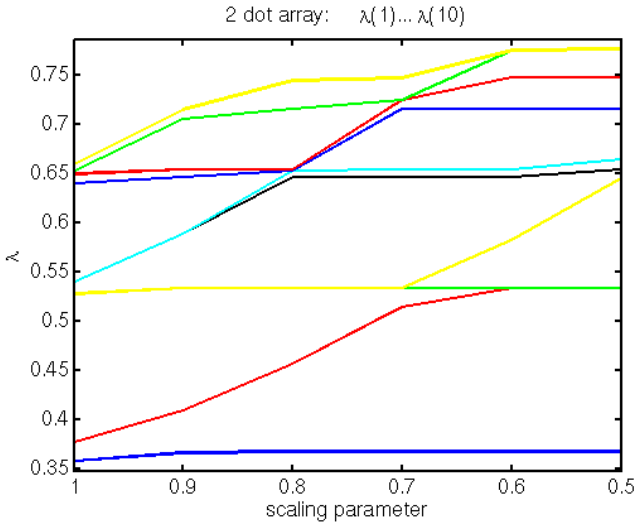

FIG. 5.7. *The energy levels of a vertically aligned array of two quantum dots at 1 nm distance, the lower one scaled, in dependence of the scaling parameter*

only one more than for a single dot. In fact, all but one the envelope functions live on the larger dot, with the exception of the one additional state introduced by the array structure as the consequence of the simplicity of the ground state. Furthermore, this becomes the 4th instead of 2nd energy level owing to the difference in volume of the two dots.

Summarizing, generally the energy levels are very sensitive to scaling one of the dots, but it remains secondary which one of them has been scaled. Nevertheless, the symmetry with the respect to the perturbation gets lost much quicker than in the case of

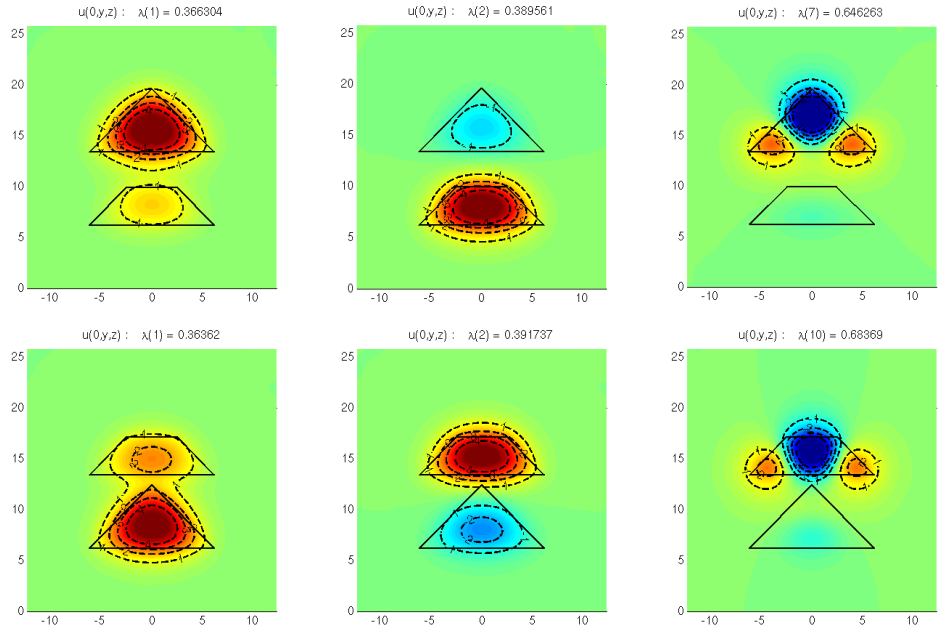

FIG. 5.8. *Envelope functions of a vertically aligned array of two dots at 1 nm distance, one of them truncated at the height of 0.4 height of the dot, the lower dot (first row), the upper dot (second row)*

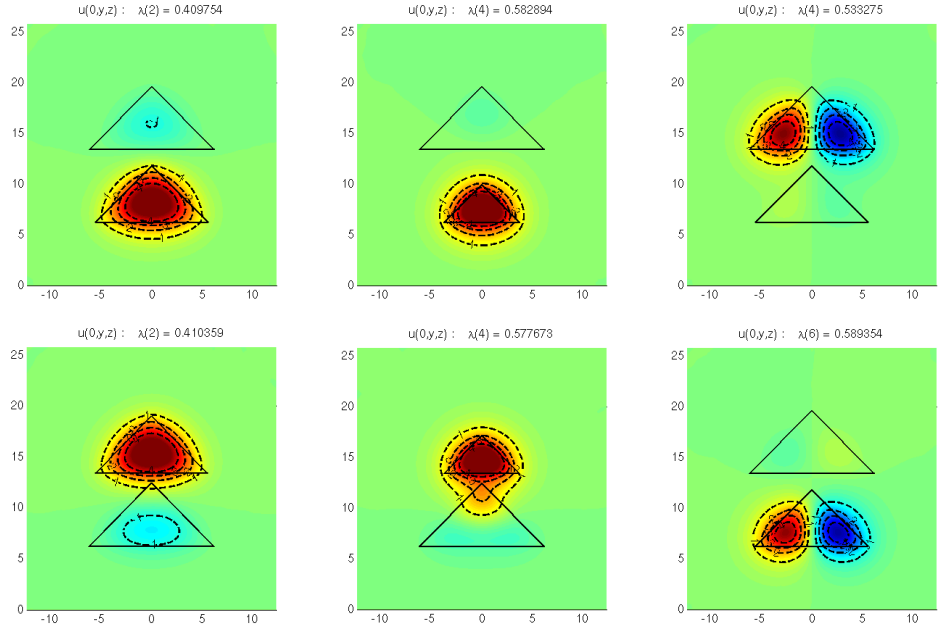

FIG. 5.9. *Envelope functions of a vertically aligned array of two dots at 1 nm distance, leftmost column: 2nd state for the lower and upper dot scaled by 0.9, respectively, middle column: 4th state for dots scaled by 0.6, rightmost column: 4th and 6th states for lower dot scaled by 0.9*

the less sensitive perturbation like truncation of the top of the pyramid. Again, all discussed perturbations have the same effect in the presence of wetting layers.

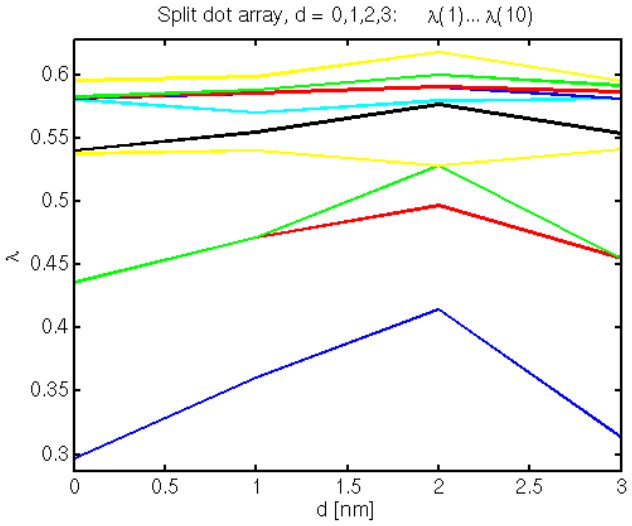

FIG. 5.10. *Energy levels of vertically coupling quantum dots in dependence of the parameter d*

Finally, we examine the four stages of formation of vertically coupled quantum dots shown in Figure 2.1. In the following we consider the structures in order of growing distance d between the components. For $d = 0$ the structure is actually a single quantum dot with the additional wetting layer cutting through it. From the former experience with the wetting layer we expect the additional wetting layer to lower the energy levels even more and this is in fact the case. The ground level and the first excited state are smaller by about 5%. There are 43 confined states, 16 more than in the case of a single dot on wetting layer. Compared to the dot we observe interchanging of some energy levels too e.g. (4/5th and 7/8,9th). Inferring from the Figure 5.11 this is due to the irregular volume increase, which has different impact on individual energy levels. Likewise, as for a dot, the envelope functions corresponding to the energy levels strarting from the 6th onwards also extend to here both wetting layers.

The two following structures $d = 1, 2$ can be interpreted as an array of two perturbed dots, the lower one with truncated tip and the other scaled in such a way, that they form a split dot. From the discussion above we can expect quite an irregular behavior due to diversity of structure features such as the presence of the wetting layer and an array assembly along with the extensive perturbation of both compounds. For the ground state for $d = 1$ we observe a localization to the lower dot while for $d = 2$ to the upper one. The further 5 energy levels for d = 1 are quite localized and therefore corespond to those of a single dot with the exception of the 4th state exhibiting an interesting splitting between the dots. For $d = 2$ the 2nd energy level is the extra "array one" and the 3rd is double. There is no clear 4th dot state and the 5th and 6th are swapped regarding $d = 1$ (cf. Figure 5.10). In general for $d = 1$ the states tend to be more confined to the lower dot, with some exceptions of splitting between the dots, while for $d = 2$ the states starting with the 3rd one more uniformely distribute across the whole structure. In both cases there are 43 confined states as for d = 0.

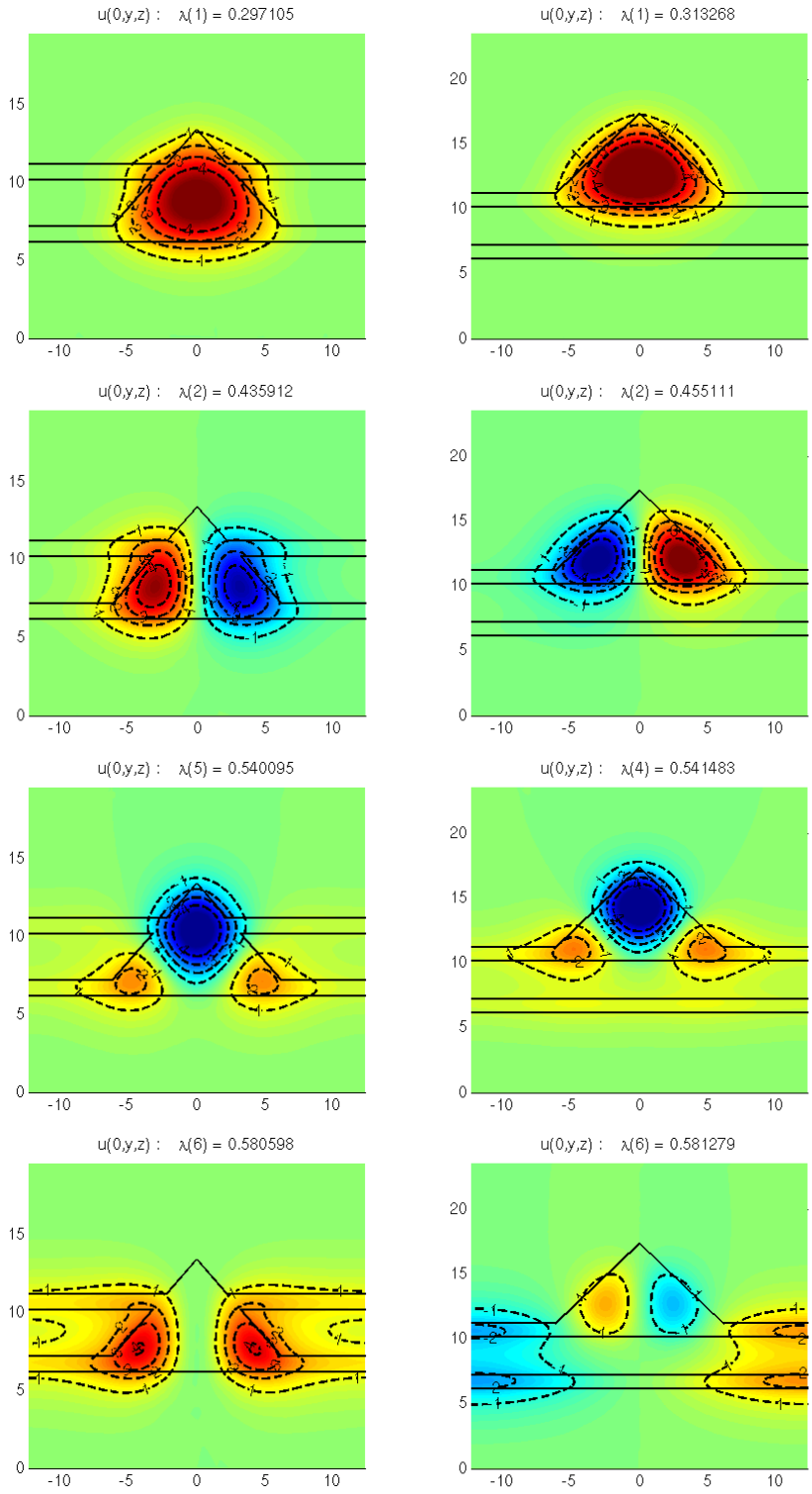

FIG. 5.11. *Envelope functions of a vertically coupled quantum dots for* $d = 0$ *in the left column,* $d = 3$ *in the right column*

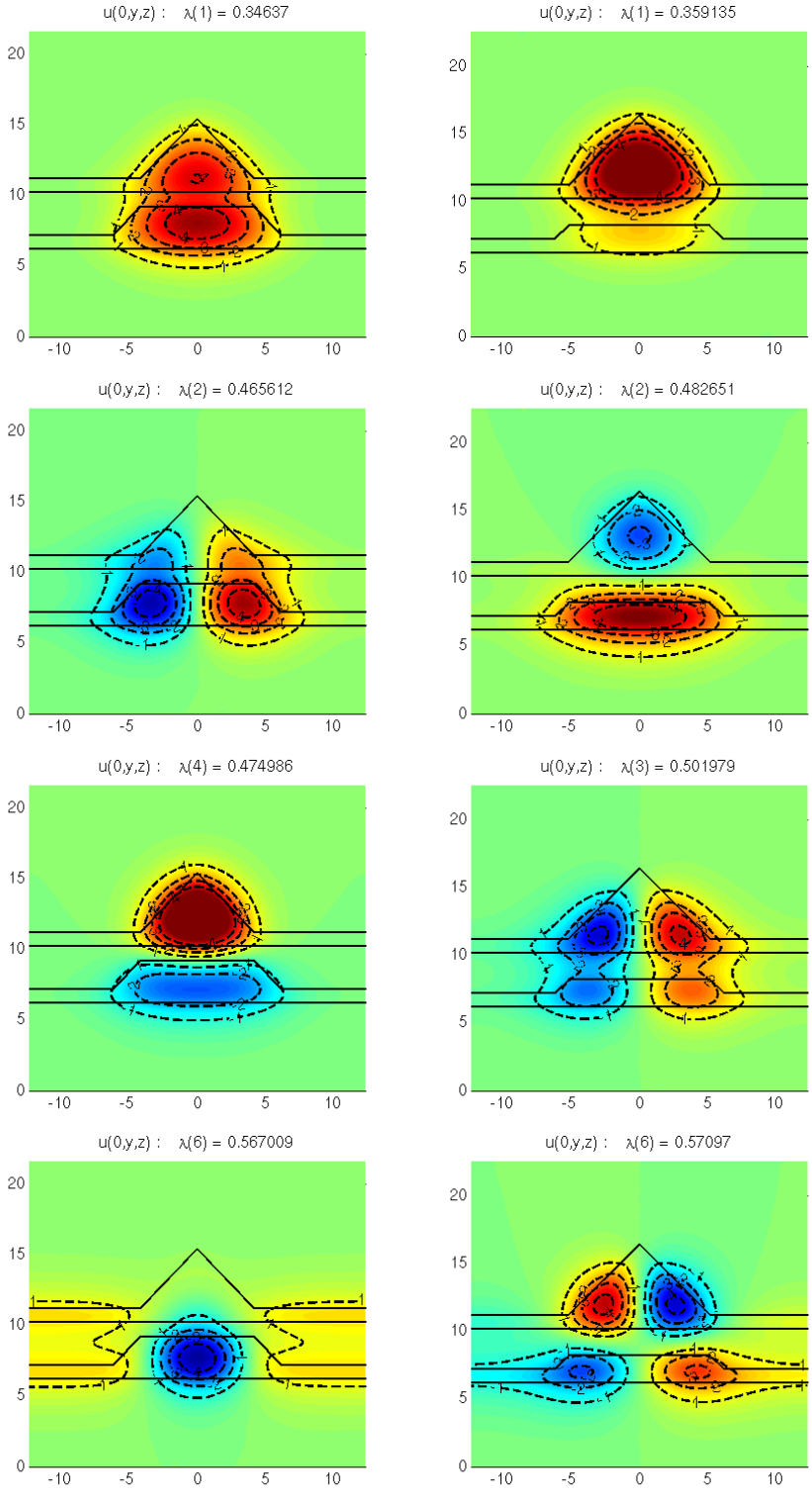

FIG. 5.12. *Envelope functions of a vertically coupled quantum dots for* $d = 1$ *in the left column,* $d = 2$ *in the right column*

The last structure is an array composed of a pure wetting layer and a dot on a wetting layer. As expected, the first five energy levels are localized to the dot. Once the envelope functions start to live on the wetting layer the array structure comes to play. The second wetting layer lowers the energy levels which also live on it. 6th pure dot, becomes 9th structure since it is quite localized therefore larger. Here we have 45 confined states.
Summarizing, as a single dot on wetting layer has 27 and hence the well separated array two times as many confined states which reduce to 52 with disceasing the distance between the dots. The vertically coupled dots structures have 43 up to 45 confined states. From the further reduction of the number of confined states we infer, that the coupling is much larger for all vertically coupled structures than it was for an original array. As expected, the coupling for $d = 0$ is slightly smaller than for the others, but the main difference lies in the shape of the eigenfunctions and how they distribute over the structure. In general it is difficult to derive some systematical behavior. This irregularity is also visible in the plot showing the dependence of the energy levels on d.

6. Conclusions. We applied the Nonlinear Arnoldi method to various nanostuctures containing quantum dots. We found that it is an efficient tool for solving the problems in the band structure calculation. The method easily coped with badly separated and even multiple eigenvalues. We provided numerical evidence that the nonlinear model is necessary to correctly capture the confined energy levels. Our simulations showed that the wetting layer lowers the energy levels and introduces many additional confined states. Once the energy levels reach the ground state of the quantum well the envelope functions expand to the wetting layer and the confinement for the excited states wares of with the increasing thickness of the wetting layer. Further, we found that the dots in an array are coupled provided their distance is sufficiently small. We demonstrated, that change of shape of one of the compound dots like truncation of its tip must be already larger to have an effect, but then we encounter eigenstate localization for some of the energy levels. For smaller perturbations the system behaves similarly to the coupled unperturbed system. If the dots vary in size, already a quite small discrepancy has the effect of localizing the eigenstates, so that the eigenstates tend towards the states of a single dot. This effect gets amplified with the increasing size difference. All these phenomena come to bear in vertically coupled dot structures and from all our examples they exhibited the strongest coupling of energy states. In all coupled structures we encountered energy level interchange.

For future research it would be interesting to incorporate more complex models including, e.g. more bands, the anisotropy in the conduction band or spin orbit splitting. Another absorbing issue is the behavior of nanostructures in the presence of magnetic field. In all these situations reliably and efficient algorithms need to be tailored.

REFERENCES

[1] G. Bastard. *Wave Mechanics Applied to Semiconductor Heterostructures*. Les editions de physique, Les Ulis Cedex, 1988.
[2] T. Betcke and H. Voss. A Jacobi–Davidson–type projection method for nonlinear eigenvalue problems. *Future Generation Computer Systems*, 20(3):363 – 372, 2004.
[3] S.L. Chuang. *Physics of Optoelectronic Devices*. John Wiley & Sons, New York, 1995.
[4] FEMLAB, Version 3.1. COMSOL, Inc., Burlington, MA, USA, 2004.

[5] I. Filikhin, E. Deyneka, G. Melikian, and B. Vlahovic. Electron states of semiconductor quantum ring with geometry and size variations. *Molecular Simulation*, 31:779 – 785, 2005.
[6] I. Filikhin, E. Deyneka, and B. Vlahovic. Energy dependent effective mass model of InAs/GaAs quantum ring. *Model.Simul.Mater.Sci.Eng.*, 12:1121 – 1130, 2004.
[7] L. R. C. Fonseca, J. L. Jimenez, J. P. Leburton Electronic coupling in InAs/GaAs self–assembled stacked double–quantum–dot systems *Physical Review B*, 58:9955 – 9960, 1998.
[8] P. Harrison. *Quantum Wells, Wires and Dots. Theoretical and Computational Physics.* John Wiley & Sons, Chicester, 2000.
[9] T.–M. Hwang, W.–W. Lin, J.–L. Liu, and W. Wang. Jacobi–Davidson methods for cubic eigenvalue problems. *Numer.Lin.Alg.Appl.*, 12:605 – 624, 2005.
[10] T.–M. Hwang, W.–W. Lin, W.–C. Wang, and W. Wang. Numerical simulation of three dimensional quantum dot. *J.Comput.Phys.*, 196:208 – 232, 2004.
[11] T.–M. Hwang, W. Wang. Energy States of Vertically Aligned Quantum Dot Array with Nonparabolic Effective Mass. *Comput.Math.Appl*, 196:208 – 232, 2004.
[12] N. N. Ledentsov, et al Direct formation of the vertically coupled quantum dots in Stranski-Krastanov growth *Physical Review B*, 54:8743 – 8750, 1996.
[13] Y. Li. Numerical calculation of electronic structure for three-dimensional nanoscale semiconductor quantum dots and rings. *J. Comput. Electronics*, 2:49 – 57, 2003. *J. Comput. Electronics*, 2:49 – 57, 2003.
[14] Y. Li, O. Voskoboynikov, C.P. Lee, and S.M. Sze. Computer simulation of electron energy level for different shape InAs/GaAs semiconductor quantum dots. *Comput.Phys.Comm.*, 141:66 – 72, 2001.
[15] Y. Li, O. Voskoboynikov, C.P. Lee, and S.M. Sze. Calculation of induced electron states in the three–dimensional semiconductor artificial molecules *Comput.Phys.Comm.*, 147:209 – 213, 2002.
[16] M. Markiewicz, H. Voss Electronic States in Three Dimensional Quantum Dot/Wetting Layer Structures *ICCSA* , LNCS 3980, 684 – 693, 2006
[17] R.V. Melnik and M. Willatzen. Modelling coupled motion of electrons in quantum dots with wetting layers. In *Proceedings of the 5th Internat.Conference on Modelling and Simulation of Microsystems, MSM 2002*, pages 506 – 509, Puerto Rico, USA, 2002.
[18] R.V. Melnik and M. Willatzen. Bandstructures of conical quantum dots with wetting layers. *Nanotechnology*, 15:1 – 8, 2004.
[19] R.V. Melnik and K.N. Zotsenko. Computations of coupled electronic states in quantum dot/wetting layer cylindrical structures. In P.M.A. Sloot, D. Abramson, A.V. Bogdanov, J.J. Dongarra, A.Y. Zomaya, and Y.E. Gorbatchev, editors, *Computational Science – ICCS 2002, 3rd International Conference,Proceedings, Part III*, volume 2659 of *Lecture Notes in Computer Science*, pages 343–349, Berlin, 2003. Springer Verlag.
[20] R.V. Melnik and K.N. Zotsenko. Finite element analysis of coupled electronic states in quantum dot nanostructures. *Modelling Simul. Mater. Sci. Eng.*, 12:465 – 477, 2004.
[21] A. Neumaier. Residual inverse iteration for the nonlinear eigenvalue problem. *SIAM J. Numer. Anal.*, 22:914 – 923, 1985.
[22] H. Voss. Initializing iterative projection methods for rational symmetric eigenproblems. In *Online Proceedings of the Dagstuhl Seminar Theoretical and Computational Aspects of Matrix Algorithms, Schloss Dagstuhl 2003*, ftp://ftp.dagstuhl.de/pub/Proceedings/03/03421/03421.VoszHeinrich.Other.pdf, 2003.
[23] H. Voss. An Arnoldi method for nonlinear eigenvalue problems. *BIT Numerical Mathematics*, 44:387 – 401, 2004.
[24] H. Voss. Electron energy level calculation for quantum dots. Comput. Phys. Comm. 174: 441–446, 2006
[25] H. Voss. A rational eigenvalue problem governing relevant energy states of a quantum dots. doi:10.1016/j.jcp.2006.01.034
[26] H. Voss. A New Justification of the Jacobi-Davidson Method for Large Eigenproblems submitted to Lin. Alg. Appl.